Indirect power control of grid-connected photovoltaic system using fuzzy control with a three-level inverter

Hassan Essakhi, Sadik Farhat, Yahya Dbaghi, Diyae Daou

Laboratory of Engineering Sciences and Energy Management (LASIME), Department of Electrical Engineering,
Higher School of Technology, Ibn Zohr University, Agadir, Morocco

Article Info	ABSTRACT
	This paper proposes an enhanced study of a photovoltaic generator (PVG) connected to the grid. A fuzzy maximum power point tracking (MPPT) is used to extract maximum power. The control strategy adopted gives the possibility to control separately the active and reactive power. the voltage control at the input of the three levels inverter allows fixing the reference currents in the DQ frame to control indirectly the power injected into the grid. The use of a three-level neutral point clamped voltage source inverter (3L-NPC-VSI) with space vector pulse width modulation (SVPWM) control and the RL filter allows to have a quality current and voltage wave with a minimum total harmonic distortion (THD). The simulation results on MATLAB/Simulink confirm the performance of this proposed strategy in the steady-state with high efficiency.

Corresponding Author:

Hassan Essakhi
Laboratory of Engineering Sciences and Energy Management (LASIME)
Department of Electrical Engineering, Higher School of Technology, Ibn Zohr University
B.P. 33/S, Agadir 80000, Morocco
Email: hassan.essakhi@edu.uiz.ac.ma

1. INTRODUCTION

Morocco has launched a national energy strategy whose objective is to produce in 2030 at least 52% of electricity from renewable energy sources (RES) such as solar PV and wind energy and has progressively started to open up the production of electricity from RES and market it to consumers connected to the grid. However, the RES are intermittent and unpredictable sources because they are dependent on weather conditions. Thus, the integration of RES makes special requirements on the electricity grid in terms of quality, stability, and control of the injected power.

The participation of Photovoltaics in energy generation is increased because of the negative environmental effects of conventional energy sources. In this context several publications on PV systems have been issued in recent years, most of the research is focused on the production side or on the grid injection side, or both to improve the overall efficiency. The first challenge is the extraction of maximum power from the PVs, in fact, several algorithms for Maximum power point tracking (MPPT) are proposed which can be classified into two types: classical algorithms and advanced algorithms. Among the most popular classical methods are the "perturb and observe" algorithm (P&O) and incremental conductance (IC) algorithm [1]-[3]. Farhat *et al.* [4] studied the effectiveness of the two techniques; (P&O) and (IC) and concluded that the (IC) offers a slight advantage in terms of response time dynamic. However, the measured power point oscillates around the MPP due to variations in the duty cycle of the DC/DC converter using a fixed step. Some researchers have tried to develop these methods by varying the step size [5]-[8]. Artificial intelligence techniques are introduced to optimize the dynamics of the PPM search such as a fuzzy logic

controller (FLC) [9], [10] and artificial neural networks (ANN) presented in [11], [12], these advanced methods have demonstrated better performance. The power injection is controlled by the grid-connected inverter. Hence, much research on the inverter control has been done. Noguchi *et al.* [13] suggests a method known as direct power control (DTC) which is based on the direct control of active (P) and reactive (Q) power without a current loop. Nevertheless, this technique has a low capacity to control the power P and Q simultaneously and the switching frequency is not constant [14]. To solve this problem many researchers have proposed various developed approaches [15]. Another technique based on indirect (P) and (Q) control by current control in the d-q frame is named voltage-oriented control (VOC) [16], [17]. VOC is considered to be more efficient due to energy loss and current distortion than DTC [16], [18].

This work presents the modeling and simulation of a 61 KW PV system whose objective is to improve the efficiency of extracting maximum power and the control of the power injected into the grid with a better quality of voltages and currents with a low total harmonic distortion (THD). The present study is structured as follows: section 2 will be devoted to the proposed method. The simulation results are detailed in section 3. Finally, section 4 concludes with a summary.

2. METHOD

To validate our approach, we based on the diagram in Figure 1. A fuzzy logic based MPPT is proposed to act on a boost to extract the maximum power. the VOC method with PI controllers is adopted in this paper for the grid side we have chosen a Three-level neutral point clamped voltage source inverter (3L-NPC-VSI) controlled by the SVPWM strategy with an RL filter ensuring the elimination of harmonics.
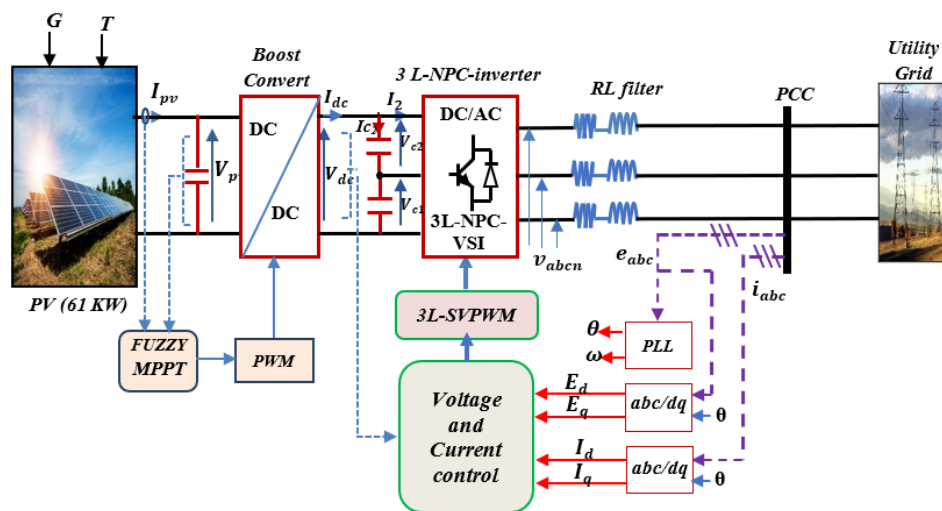

Figure 1. Principle diagram of the proposed control for the PV conversion system

2.1. DC side modeling and control
2.1.1. Photovoltaic generator (PVG) Modeling

To set up the GPV model, we must first establish the electrical circuit equivalent. For several years great effort has been devoted to the study of mathematical models [9], [19]-[21]. For simplicity, the single-diode model as shown in Figure 2, is used in this paper. This model offers a good compromise in terms of ease and exactitude [9].

From Figure 2 it can be seen that the PV current I_{pv} is described by (1):

$$I_{pv} = I_{ph} - I_0 - I_p \tag{1}$$

where: I_{pv}: PV generator current supplied (A), I_{ph} is the photocurrent that mostly depends on the solar irradiance and cell's temperature, I_0 is the diode current (A) and I_p is the current leak in a parallel resistor (A).

The V_{pv}-I_{pv} characteristic of the PV array can be computed by the following (2) [9]:

$$I_{pv} = N_p \cdot I_{ph} - I_s \left[exp\left(\frac{q\left(\frac{V_{pv}}{N_s} + \frac{I_{pv} \cdot R_s}{N_p}\right)}{K \cdot T_c \cdot A} - 1 \right) - \left(\frac{\frac{N_p \cdot V_{pv}}{N_s} + I_{pv} \cdot R_s}{R_p} \right) \right] \qquad (2)$$

where N_p is the cell number parallel of the module, N_s is the cell number in series, I_s is the cell's saturation current, q is the electron charge (1.6×10^{-19} C), K is the Boltzmann constant (1.38×10^{-23} J/K), T_c: is a cell temperature in kelvin (K), A is the ideal factor dependent on PV technology, R_s: is a series resistance (Ω), and R_P is the parallel resistor.
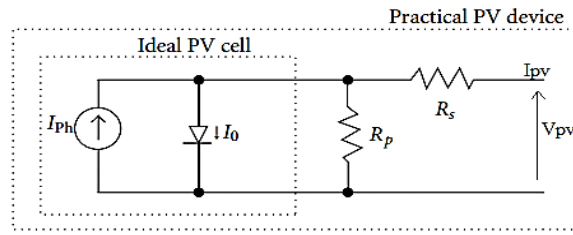

Figure 2. Equivalent model of PV cell

To fully understand the electrical performances of the PV array, we simulated the model using MATLAB/Simulink software. The characteristics of the solar panel used to validate our proposed method are shown in Table 1.

Table 1. Parameters of PV module

PV module parameter	Value
Maximum Power (W)	305.226
Celles per module (Ncell)	96
Open circuit voltage Voc (V)	64.2
Short-circuit current Isc (A)	5.96
Voltage at maximum power point Vmp (V)	54.7
Current at maximum power point Imp (A)	5.58
Temperature coefficient of Voc (%/deg.C)	-0.2727
Temperature coefficient of Isc (%/deg.C)	0.061745

To get high power levels, the PV array is composed of strings of PV modules collected in parallel. Each string consists of modules connected in series. in our case, we used a PV array composed of 40 parallel strings and 5 series-connected modules per string. To understand the performance of the photovoltaic array we have plotted with MATLAB/Simulink as shown in Figure 3 the I-V and P-V characteristics under different irradiations values at a set temperature of 25 °C. From Figures 3(a) and (b), it can be seen that the power characteristic of the PV generator has a maximum power point MPP and the position of the MPP is affected by the climatic conditions (solar irradiation and temperature) of the cells. For irradiation of $G = 1kW/m^2$ and T=25 °C, we see that the maximum power point corresponds to $P_{mpp} = 61$ kW with $V_{mpp} = 273$ V and $I_{mpp} = 223$ A.
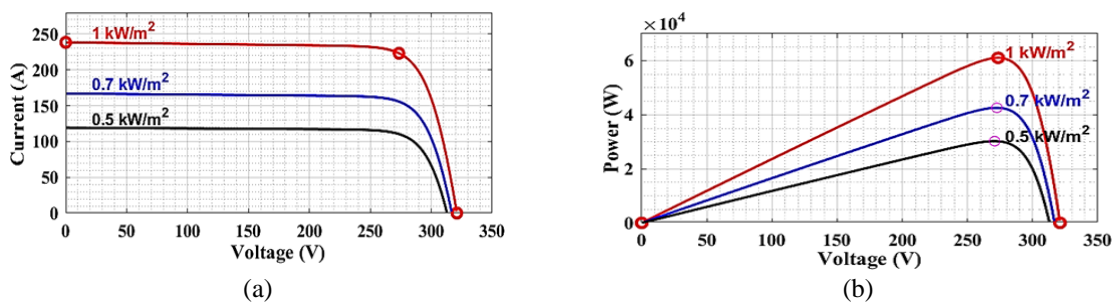

(a)

(b)

Figure 3. Influence of irradiation G at temperature T=25 °C on I-V, (a) P-V and (b) characteristics

2.1.2. MPPT control algorithm

In the published literature, we can find different types of algorithms allowing the search for the maximum power point [22]. The MPPT control must have a high level of simplicity, low power consumption, and low cost. The methods developed until now can be divided into two classes: artificial intelligence methods and conventional methods. In our study we will focus on two control algorithms: the classical incremental conductance (IC) [23]-[25] and proposed fuzzy logic (FL).

a. Proposed fuzzy logic controller (FLC)

As can be seen from Figure 4, the proposed FLC has two inputs, the error (E) and the change of error (CE) with the output ΔD which is used to vary the duty cycle D of the boost converter. The (E), (CE), and (ΔD) can be computed at sample times k by the following equations [9], [26], [27]:

$$E(k) = \frac{P_{pv}(k) - P_{pv}(k-1)}{V_{pv}(k) - V_{pv}(k-1)} \tag{3}$$

$$CE(k) = E(k) - E(k-1) \tag{4}$$

$$D(k) = D(k-1) + \Delta D(k) \tag{5}$$

where the $P_{pv}(k)$, and $V_{pv}(k)$ are the output power and voltage of the PVG at the time k respectively. The FLC's variables (E, CE, and ΔD) are transformed into linguistic variables. In this study, the universe of discourse (UOD) is divided into five fuzzy sets very low (VL), low (L), zeros (ZE), high (H), and very high (VH). In Figure 5 the membership functions as can be seen from Figures 5(a)-(c) triangular membership functions are selected for all states, except for the extremities of each function where the trapezoidal form is used. The inference engine is made up of a fuzzy set of rules. The development of the fuzzy rules is based on the use of the Mamdani strategy.
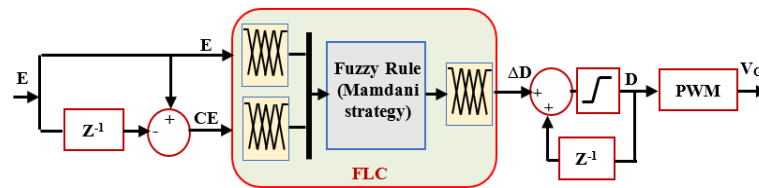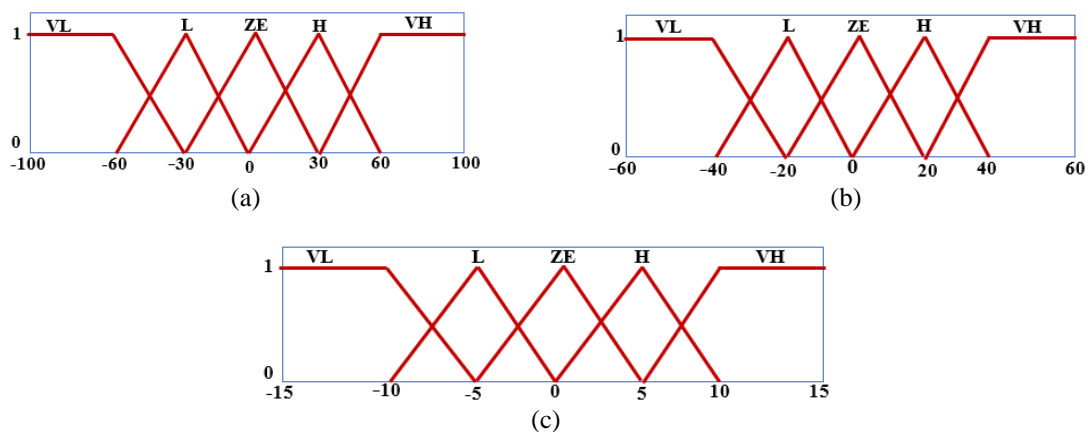

Figure 4. Structure of FLC MPPT

Figure 5. The membership functions: (a) input E, (b) input CE, and (c) output ΔD

To illustrate this method (Max-Min), Table 2 shows 25 rules used in our study. After combining the rules, the fuzzy value must be transformed into a numerical value at the output. The most popular technique is the centroid method, where we look for the center of gravity (CG) of the fuzzy set defined as:

$$\Delta D_{CG} = \left(\sum_{i=1}^{n} \mu(x_i).x_i\right) / \left(\sum_{i=1}^{n} \mu(x_i)\right) \qquad (6)$$

where $\mu(x_i)$ is the membership value for a point x_i in (UOD), and n represents the number of rules.

Table 2. Proposed fuzzy rule table

CE E	VL	L	ZE	H	VH
VL	ZE	ZE	VL	VL	VL
L	ZE	ZE	L	L	L
ZE	L	ZE	ZE	ZE	H
H	H	H	H	ZE	ZE
VH	VH	VH	VH	ZE	ZE

2.2. AC side modelling and control

In this section we focus on the modelling and control of a grid-connected PVG system, whose main objective is to study the behavior of the PV cells and to improve their performance by ensuring the extraction of the maximum power and the control of the inverter. The energy produced by the PV modules must be converted to be usable. This conversion is done through an inverter that converts DC to AC current synchronized with the grid, with the correct amplitude, frequency, a power factor equal 0 and minimum THD in conformity with the norms in order to guarantee the power quality at the point of common coupling (PCC).

2.2.1. 3L-NPC-VSI with SVPWM

In this paper a (3L-NPC-VSI) shown in Figure 6 is suggested, this type of inverter offers many benefits compared to the classical two-level inverter 2L-VSI such as reduced voltage fluctuations (dv/dt), a minimizing of the THD, in addition, the semiconductors power components block a reverse voltage equal to only $V_{DC}/2$, and gives a compromise between the efficiency and the simplicity of control [28]-[30].

As can be seen from Figure 6 each arm is composed of four switches connected in series and two clamped diodes and each arm of the inverter can take three states. Table 3 summarizes the output voltage (v_{io}) of a 3L-NPC inverter with different switch states of phase i with i={a,b,c} and we will express these three different states by the notation +1,0 and -1 which correspond respectively to the voltage levels $V_{dc}/2,0$ and $-V_{dc}/2$ .Thus the 3L-NPC-VSI has $3^3 = 27$ possible states. Note that some switching states are redundant and generate the same voltage vector, so we have only 19 different voltage vectors V_0 to V_{18} . This is illustrated in Figure 7. For example, the V_0 vector can be generated by three different switching states :(1,1,1), (0,0,0), (-1, -1, -1).
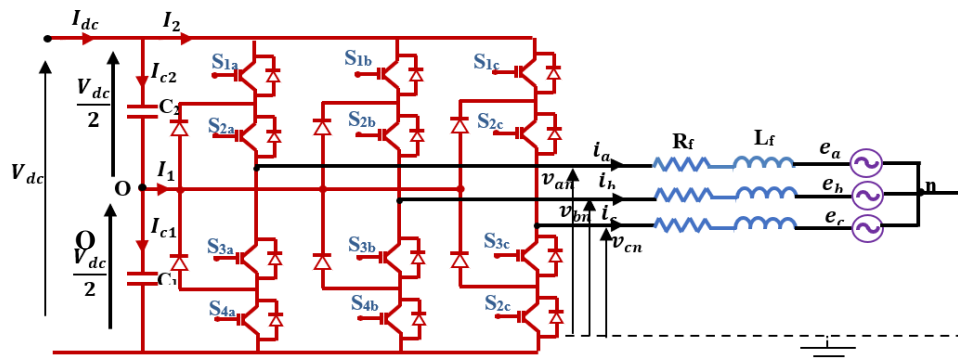

Figure 6. 3L-NPC-VSI topology connected to the grid

Table 3. The possible switching states for each arm in 3L-NPC-VSI

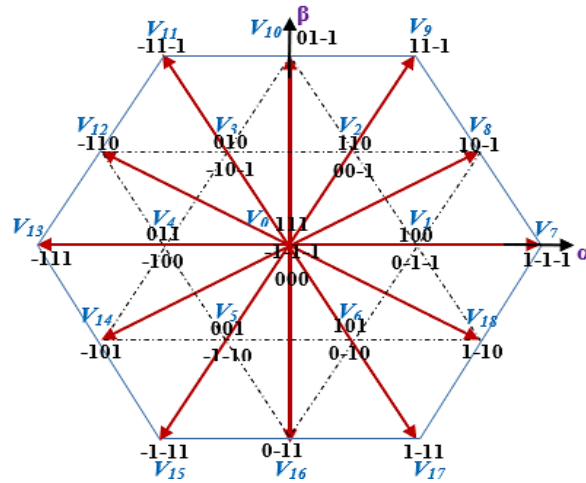| Switch states i= {a, b, c} $\{S_{1i}S_{2i}S_{3i}\,S_{3i}\}$	Output voltage v_{io}	
1100	$V_{dc}/2$	(1)
0110	0	(0)
0011	$-V_{dc}/2$	(-1)

Figure 7. 3-level inverter voltage vectors

2.2.2. Vector control strategy for 3L-NPC-VSI

The technique used in our paper is known as VOC (voltage-oriented control). This method provides high dynamic and static performance through internal current control loops [17]. This technique is based on the transformation between the stationary reference frame abc and the synchronous frame d-q using the park transformation. Thus, the variables are DC components in steady-state. The principle consists in measuring the grid voltage and detecting its angle θ for the orientation voltage in the d q axes using the phase looked loop (PLL) shown in Figure 8. This loop assures the phase tracking of the direct component of the voltage, to eliminate the quadrature component ($E_q = 0$).
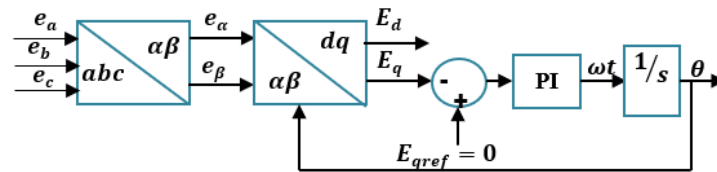

Figure 8. Block diagram of the PLL used for the detection of θ

Based on Figure 6, the inverter output voltage is calculated using the Park transformation, and considering that the system is balanced, the homopolar part is zero and the model is reduced to two components only. Considering that the d axis is in phase with the voltage grid (the E_d component and in phase with the voltage e_a). Thus, the expressions for the d and q components of the output voltages of the inverter become:

$$\begin{bmatrix} V_d \\ V_q \end{bmatrix} = \begin{bmatrix} R_f & -L_f\omega \\ L_f\omega & R_f \end{bmatrix} \begin{bmatrix} I_d \\ I_q \end{bmatrix} + L_f \frac{d}{dt} \begin{bmatrix} I_d \\ I_q \end{bmatrix} + \begin{bmatrix} E_d \\ E_q \end{bmatrix} \tag{7}$$

where: V_d and V_q are the direct and quadratic components of the voltages at the output of the inverter; $E_d, E_q, I_d,$ and I_d are the components of the grid voltages and currents in the d-q plane, respectively; $\omega = 2\pi f$ ($f = 50\ Hz$) corresponding to the pulsation of the three-phase grid currents; L is a filter inductance and R is a filter resistor. We can notice in (7), that there is a coupling between the axes of the park transformation, so a change on I_d provokes a change on I_q and vice versa., a decoupled control for (7) must be applied.

2.2.3. Indirect power control

The control of the active and reactive powers to be injected is done through the internal loops of current regulation of the inverter, the relation between power and current is linear. To calculate the PI

correctors, the decoupled model in the park reference frame must be taken into account. To do this, we propose to regulate I_d and I_q not by V_d and V_q but by γ_d and γ_d. Thus, the following equation is obtained:

$$\begin{cases} \gamma_d = V_d + \left(L_f \omega I_q - E_d\right) = L_f \frac{dI_d}{dt} + R_f I_d \\ \gamma_q = V_q - \left(L_f \omega I_d + E_q\right) = L_f \frac{dI_q}{dt} + R_f I_q \end{cases} \tag{8}$$

where γ_d and γ_d are the output signals of the current regulators.

It is, therefore, possible to control the I_d and I_q by acting on γ_d and γ_d independently. So, it is easy to size the PI controller's parameters. The expression of active and reactive powers is given in the park reference frame by the relation (9).

$$\begin{cases} P = 1.5(E_d I_d + E_q I_q) \\ Q = 1.5(E_q I_d - E_d I_q) \end{cases} \tag{9}$$

As we suppose that the d axis is synchronized with the grid voltage ($E_d = E_m = 220.\sqrt{2}$ and $E_q = 0$), where E_m is the maximum grid voltage value between phase and neutral. Thus in (10) can be simplified:

$$\begin{cases} P = 1,5. E_d. I_d = V_{dc} I_{dc} \\ Q = -1,5. E_d. I_q \end{cases} \tag{10}$$

therefore, from the relation (10), the control of the (P) and (Q) can be realized respectively by the currents I_d and I_q independently and indirectly. A PI regulator is enough for this control type. The schematic diagram of this control type is given in Figure 9.

Figure 9. Diagram of the voltage-oriented control with decoupling method

3. RESULTS AND DISCUSSION

To validate the theoretical study and the efficiency of the proposed control strategy, a complete PV conversion chain structure consisting of a PVG, a boost converter, and a three-level inverter NPC connected to the grid is designed in the MATLAB/Simulink environment., where the parameters and data of the PV system module used in these simulations are given in Table 4. Two tests have been performed with different conditions. First, we tested the power production efficiency at different irradiation levels with a temperature of 25 °C and compared the two MPPT algorithms based on CI and the suggested FLC. The second test is the simulation of the proposed model with the same irradiation conditions using the offered fuzzy MPPT method, and a 3L-VSI-NPC controlled by the VOC technique with an space vector pulse width modulation (SVPWM) strategy.

3.1. Testing the power production efficiency under different irradiation levels

The simulation duration is 1.5 s and the irradiation profile adopted for our study is shown in Figure 10 and explained by the (11).

$$time = \begin{cases} [0s, 0.4s]: G = 1KW/m^2 \\ [0.4s, 0.45s]: ramp\ down\ 1\ to\ 0.5\ KW/m^2 \\ [0.4s, 0.95s]: G = 0.5\ KW/m^2 \\ [0.95s, 1s]: ramp\ up\ 0.5\ to\ 1\ KW/m^2 \\ [1s, 1.5s]: G = 1\ KW/m^2 \end{cases} \tag{11}$$

from the results presented in Figure 11, we can notice that the maximum power was extracted using the two algorithms MPPT CI and FLC. We see that both methods, CI and FLC, converge to the maximum power point MPP in steady-state. However, we observe significant oscillations around the MPP in the case of CI MPPT.On the other hand, the proposed FLC MPPT is stable and has negligible oscillations. This result is validated by Figure 12, which shows that FLC MPPT is more efficient, thus proving the effectiveness of the proposed technique.
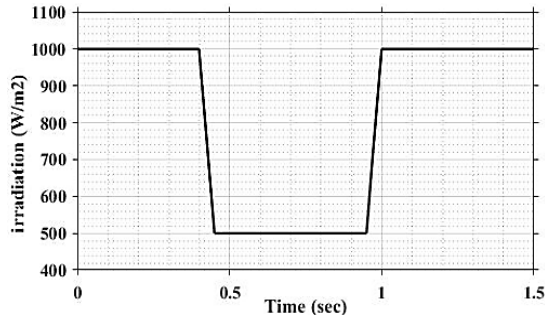
Figure 10. Irradiation profile
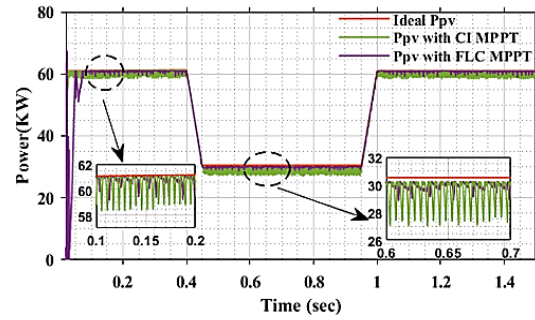
Figure 11. PV generator power response
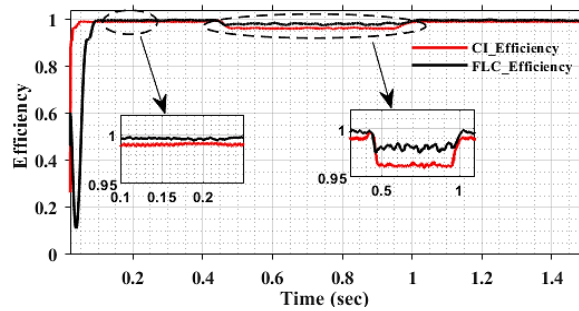
Figure 12. PVG efficiency

3.2. The control results of the grid side inverter

As can be seen from Figure 13 we notice that the DC bus voltage response is aligned with the required reference (V_{dc*}=800V) we show also a small undershoot of -10V during a ramp-down of G at 0.45s. We also note a neglected overshoot of 8V at 1s when a ramp-up of G is applied. Therefore, an overshoot of around 1.25% which is negligible, this demonstrates the performance of the PI correctors used. The successful response of DC voltage provides a reference current I_{d*} as indicated in Figure 14 which shows that the active current I_d is tracking their reference perfectly with a zero value of reactive current (I_q=0A). This means that in the steady-state, as can be seen in Figure 15, the injection of the power into the grid is done only with its active component (P=60.4 KW at G=1000 W/m^2 and P=30 KW at G=500 W/m^2), while the reactive component of this power is zero (Q=0 KVAR).

Figure 16 also indicates that during the steady-state, Grid voltage and current of phase A are in phase, which ensures a unit power factor (PF=1). Figure 17 provides the injected current, which is sinusoidal while being synchronized with the grid frequency (f=50 Hz). The quality of the sinusoidal current wave transmitted to the grid is approved by Figure 18 which presents a current THD =2.39% which conforms with the IEEE-519 standard (<5%).

Figure 19 gives the output phase to phase voltage (V_{ab}) of the 3L-VSI which contains five levels of DC voltage (V_{dc}, V_{dc}/2,0, -V_{dc}/2, -V_{dc}). Its waveform is near the sinusoid, this voltage is filtered to reduce the harmonics caused by the inverter as described in Figure 20 and Figure 21.

Figure 22 clarifies the evolution of the line-to-line voltage (V_{ab}) THD for the two topologies 2L-VSI and 3L-VSI-NPC with SVPWM control, it is evident that the THD in steady-state is stable at a value of about 1.11% for the suggested method and is lower than the THD for the 2L topology which is an average of 3.3%. A comparative analysis between the results of the two inverter types shows that the 3L-VSI configuration offers higher performance while reducing the THD as much as possible.
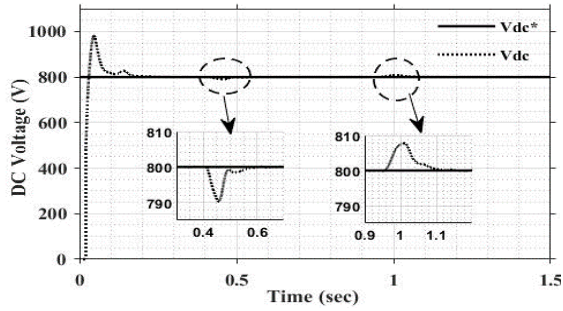
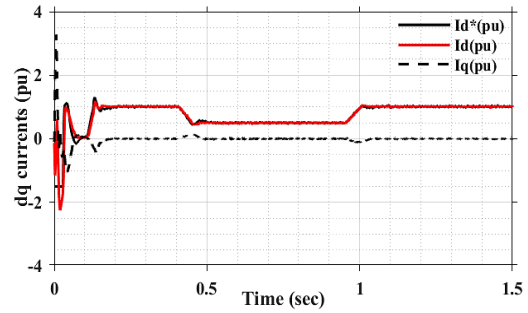Figure 13. DC bus voltage response

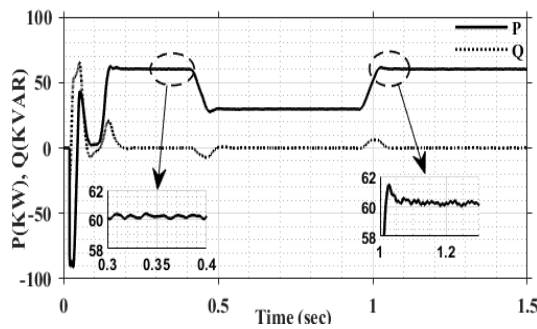Figure 14. The dq currents and d current reference in (pu) response

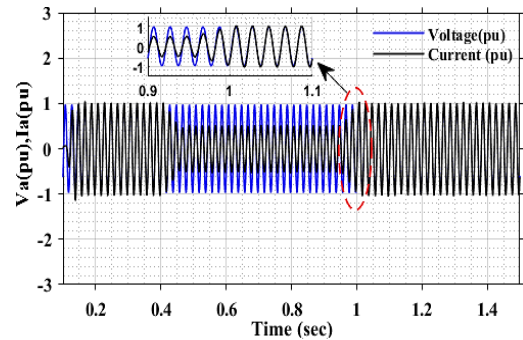Figure 15. Active and reactive power injected into the grid

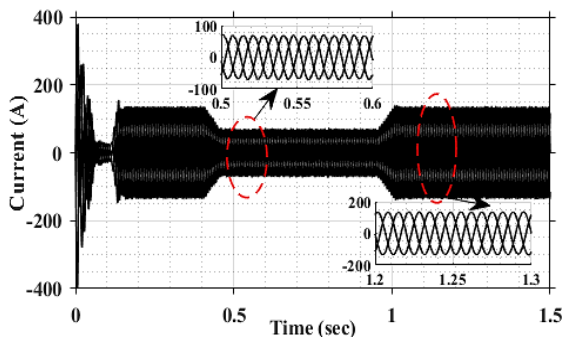Figure 16. Grid voltage and current of phase A (pu)

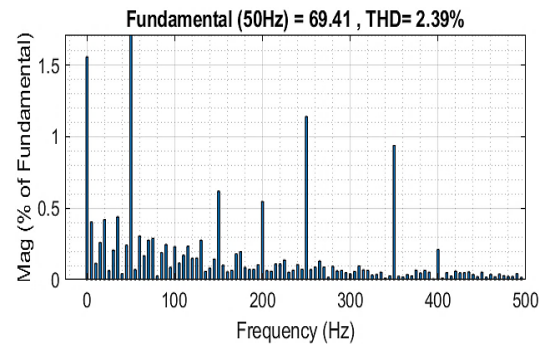Figure 17. 3-phase line currents injected into the grid with 3L-VSI-NPC

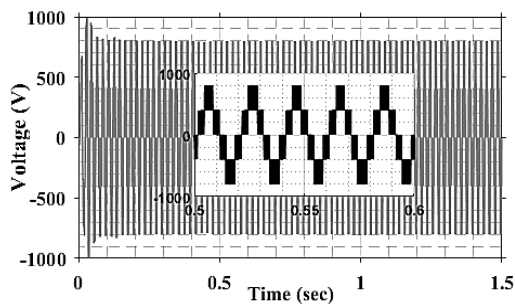Figure 18. current injected FFT analysis with proposed method

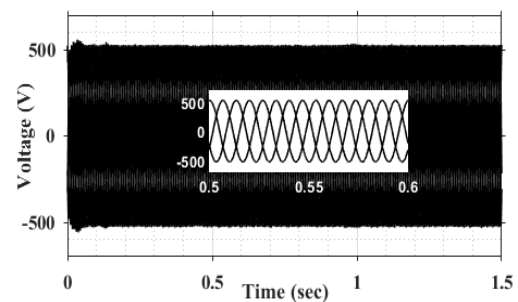Figure 19. Line to line voltage (V_{ab}) at the inverter output with 3L-VSI-NPC
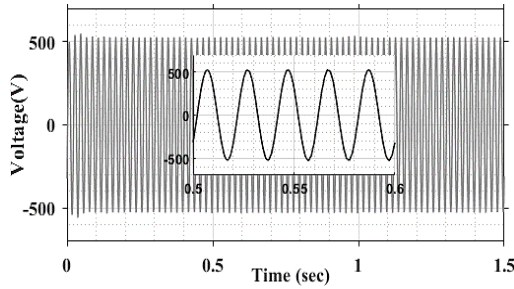

Figure 20. Three-phase voltages at the filter output with 3L-VSI-NPC

Figure 21. Fundamental line to line voltage (V_{ab}) at the Filter output with 3L-VSI-NPC
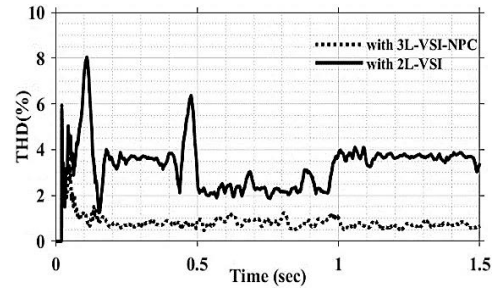
Figure 22. THD (%) line to line voltage (V_{ab}) at PCC

Table 4. Proposed system parameters

Variable	Symbol	Value
Peak output power	Pmax	61 Kw
Boost inductor	L_B	5 mH
Boost capacitor	C_B	100 μF
Boost switching frequency	f_B	5 Khz
DC link	V_{DC}	800 V
DC-Link capacitor	C	1200 μF
Inverter switching frequency	f_I	6 Khz
DC controller parameters	K_{P2}, K_{I2}	20-800
Current controller parameters	K_{P1}, K_{I1}	0.3-20
Filter inductor	L_f	2.4 mH
Filter resistor	R_f	0.001 Ω
Grid line to line voltage	V_{ab}	380 V (rms)
Grid frequency	f	50 Hz

4.   CONCLUSION

In this paper, we have proposed a more efficient control approach for a grid-connected photovoltaic system under different irradiation levels. The goal of the suggested control method is to extract the maximum power and indirect regulation of the active and reactive power injected into the electrical network while regulating the DC bus voltage by ensuring that the two regulation loops (P and Q) are completely decoupled and independent and to inject a sinusoidal current into the network with a unit power factor and an optimal THD that satisfies the standard. For this purpose, an MPPT algorithm based on fuzzy logic is proposed to act on the boost duty cycle to obtain a higher power output. we have chosen a 3L three-phase inverter with NPC structure connected to the grid via an RL filter the inverter is controlled by the decoupled VOC technique with an SVPWM strategy. We have presented the simulation results under MATLAB/Simulink. The results of the different simulations prove that the suggested control model can control the power transmitted to the grid with good dynamics, a higher quality of the voltages, and injected currents with a minimum THD imposed by the standards.

REFERENCES

[1]   M. A. Enany, M. A. Farahat, and A. Nasr, "Modeling and evaluation of main maximum power point tracking algorithms for photovoltaics systems," *Renew. Sustain. Energy Rev.*, vol. 58, pp. 1578–1586, May 2016, doi: 10.1016/j.rser.2015.12.356.
[2]   M. A. Abdourraziq and M. Maaroufi, "Experimental verification of the main MPPT techniques for photovoltaic system," *International Journal of Power Electronics and Drive Systems (IJPEDS)*, vol. 8, no. 1, p. 384, Mar. 2017, doi: 10.11591/ijpeds.v8.i1.pp384-391.
[3]   S. Alsadi and B. Alsayid, "Maximum power point tracking simulation for photovoltaic systems using perturb and observe algorithm," *International Journal of Engineering and Innovative Technology (IJEIT)*, vol. 2, no. 6, p. 7, 2012.
[4]   S. Farhat, R. Alaoui, A. Kahaji, L. Bouhouch, and A. Ihlal, "P&O and Incremental Conductance MPPT Implementation," *Int. Rev. Electr. Eng. IREE*, vol. 10, no. 1, p. 116, Feb. 2015, doi: 10.15866/iree.v10i1.4865.
[5]   M. Elyaqouti, S. Hakim, S. Farhat, L. Bouhouch, and A. Ihlal, "Implementation in Arduino of MPPT using variable step size P&O algorithm in PV installations," *International Journal of Power Electronics and Drive Systems (IJPEDS)*, vol. 8, no. 1, p. 434, Mar. 2017, doi: 10.11591/ijpeds.v8.i1.pp434-443.
[6]   G. Dileep and S. N. Singh, "Maximum power point tracking of solar photovoltaic system using modified perturbation and observation method," *Renew. Sustain. Energy Rev.*, vol. 50, pp. 109–129, Oct. 2015, doi: 10.1016/j.rser.2015.04.072.
[7]   N. Femia, G. Petrone, G. Spagnuolo, and M. Vitelli, "Optimization of perturb and observe maximum power point tracking method," *IEEE Trans. Power Electron.*, vol. 20, no. 4, pp. 963–973, Jul. 2005, doi: 10.1109/TPEL.2005.850975.
[8]   M. Killi and S. Samanta, "Modified perturb and observe MPPT algorithm for drift avoidance in photovoltaic systems," *IEEE Trans. Ind. Electron.*, vol. 62, no. 9, pp. 5549–5559, Sep. 2015, doi: 10.1109/TIE.2015.2407854.

[9]   H. Essakhi, S. Farhat, M. Mediouni, and Y. Dbaghi, "Improving the dynamic performances of an MPPT controller for a Photovoltaic system using fuzzy logic," in *E3S Web of Conferences*, 2021, vol. 229, doi: 10.1051/e3sconf/202122901013.

[10] D. Saravana, J. Mohammed, V. Umayal, and M. Indumathi, "Simulation of fuzzy logic control based MPPT technique for photovoltaic system," in *International Conference on Inovations in Engineering and Technology*, Sep. 2014. doi: 10.15242/IIE.E0914026.

[11] S. Farhat, R. Alaoui, A. Kahaji, and L. Bouhouch, "MPPT efficiency test by neural networks and P&O algorithm," *International Review of Electrical Engineering (IREE)*, vol. 8, no. 5, p. 8, 2013.

[12] K. Punitha, D. Devaraj, and S. Sakthivel, "Artificial neural network based modified incremental conductance algorithm for maximum power point tracking in photovoltaic system under partial shading conditions," *Energy*, vol. 62, pp. 330–340, Dec. 2013, doi: 10.1016/j.energy.2013.08.022.

[13] T. Noguchi, H. Tomiki, S. Kondo, and I. Takahashi, "Direct power control of PWM converter without power-source voltage sensors," *IEEE Trans. Ind. Appl.*, vol. 34, no. 3, pp. 473–479, Jun. 1998, doi: 10.1109/28.673716.

[14] Y. Tao, Q. Wu, L. Wang, and W. Tang, "Voltage sensorless predictive direct power control of three-phase PWM converters," *IET Power Electron.*, vol. 9, no. 5, pp. 1009–1018, Apr. 2016, doi: 10.1049/iet-pel.2014.0713.

[15] A. M. Razali, M. A. Rahman, G. George, and N. A. Rahim, "Analysis and design of new switching lookup table for virtual flux direct power control of grid-connected three-phase PWM AC–DC converter," *IEEE Trans. Ind. Appl.*, vol. 51, no. 2, pp. 1189–1200, Mar. 2015, doi: 10.1109/TIA.2014.2344503.

[16] M. P. Kazmierkowski and L. Malesani, "Current control techniques for three-phase voltage-source PWM converters: a survey," *IEEE Trans. Ind. Electron.*, vol. 45, no. 5, pp. 691–703, Oct. 1998, doi: 10.1109/41.720325.

[17] R. Kadri, J.-P. Gaubert, and G. Champenois, "An improved maximum power point tracking for photovoltaic grid-connected inverter based on voltage-oriented control," *IEEE Trans. Ind. Electron.*, vol. 58, no. 1, pp. 66–75, Jan. 2011, doi: 10.1109/TIE.2010.2044733.

[18] I. Aboudrar, S. E. Hani, H. Mediouni, and A. Aghmadi, "Modeling and robust control of a grid connected direct driven PMSG wind turbine By ADRC," *Adv. Electr. Electron. Eng.*, vol. 16, no. 4, pp. 402–413, Dec. 2018, doi: 10.15598/aeee.v16i4.2952.

[19] O. Gergaud, B. Multon, and H. B. Ahmed, "Analysis and experimental validation of various photovoltaic system models," *Electrimacs*, p. 8, 2002.

[20] G. Yadav and K. K. Jaladi, "Comparison of different parameters using single diode and double diode model of PV module in a PV-battery system using MATLAB Simulink," in *2017 14th IEEE India Council International Conference (INDICON)*, Dec. 2017, pp. 1–6. doi: 10.1109/INDICON.2017.8487608.

[21] H. Islam *et al.*, "Performance evaluation of maximum power point tracking approaches and photovoltaic systems," *Energies*, vol. 11, no. 2, p. 365, Feb. 2018, doi: 10.3390/en11020365.

[22] J. P. Ram, T. S. Babu, and N. Rajasekar, "A comprehensive review on solar PV maximum power point tracking techniques," *Renew. Sustain. Energy Rev.*, vol. 67, pp. 826–847, Jan. 2017, doi: 10.1016/j.rser.2016.09.076.

[23] M. A. G. de Brito, L. Galotto, L. P. Sampaio, G. de A. e Melo, and C. A. Canesin, "Evaluation of the main MPPT techniques for photovoltaic applications," *IEEE transactions on industrial electronics*, vol. 60, no. 3, pp. 1156–1167, Mar. 2013, doi: 10.1109/TIE.2012.2198036.

[24] H. Rezk and A. M. Eltamaly, "A comprehensive comparison of different MPPT techniques for photovoltaic systems," *Sol. Energy*, vol. 112, pp. 1–11, Feb. 2015, doi: 10.1016/j.solener.2014.11.010.

[25] J. Li and H. Wang, "A novel stand-alone PV generation system based on variable step size INC MPPT and SVPWM control," in *2009 IEEE 6th International Power Electronics and Motion Control Conference*, May 2009, pp. 2155–2160. doi: 10.1109/IPEMC.2009.5157758.

[26] R. E. Gouri, M. B. Brahim, and L. Hlou, "A comparative study of MPPT technical based on fuzzy logic and perturb observe algorithms for photovoltaic systems," *Journal of Theoretical & Applied Information Technology*, vol. 58, no. 2, p. 11, 2005.

[27] T. L. Kottas, Y. S. Boutalis, and A. D. Karlis, "New maximum power point tracker for PV arrays using fuzzy controller in close cooperation with fuzzy cognitive networks," *IEEE Trans. Energy Convers.*, vol. 21, no. 3, pp. 793–803, Sep. 2006, doi: 10.1109/TEC.2006.875430.

[28] U.-M. Choi, J.-S. Lee, and K.-B. Lee, "New modulation strategy to balance the neutral-point voltage for three-level neutral-clamped inverter systems," *IEEE Transactions on Energy Conversion*, vol. 29, no. 1, pp. 91–100, Mar. 2014, doi: 10.1109/TEC.2013.2293502.

[29] S.-J. Chee, H.-S. Kim, S.-K. Sul, and S. Ko, "Common-mode voltage reduction of three level four leg PWM converter," in *2014 IEEE Energy Conversion Congress and Exposition (ECCE)*, Sep. 2014, pp. 187–194. doi: 10.1109/ECCE.2014.6953393.

[30] E. Pouresmaeil, D. Montesinos-Miracle, and O. Gomis-Bellmunt, "Control scheme of three-level NPC inverter for integration of renewable energy resources into AC grid," *IEEE systems journal*, vol. 6, no. 2, pp. 242–253, Jun. 2012, doi: 10.1109/JSYST.2011.2162922.

BIOGRAPHIES OF AUTHORS

Hassan Essakhi ⓘ 🆂 ⓟ is a Ph.D. student in Electrical Engineering at the EST (high school of technology), Ibn Zohr University, Agadir. Teacher of Electrical Engineering, with a Bachelor (2012) in electromechanics at Higher Normal School of Technology (ENSET), Mohammadia, Morocco. And master's degree (2015) in electrical engineering at the Cadi Ayyad University in Marrakesh, Morocco. His research, in the context of national doctoral thesis, focuses on the thematic of Renewable Energies. The doctoral investigations took place in the Research Team in Engineering Sciences and Energy Management (LASIME) Agadir, Morocco. He can be contacted at email: hassan.essakhi@edu.uiz.ac.ma.

Sadik Farhat ⓘ 🇬 sc Ⓟ is Professor at higher education at the ESTA (Higher School of Technology), Ibn Zohr University, Agadir, Morocco. PhD in Electrical Engineering at Ibn Zohr University.Associate Professor (2001) in Electrical Engineering with a Bachelor (1996) in electronics in Higher Normal School of Technology (ENSET), Rabat, Morocco and a post graduate degree in 2007, of Energy and Environment in the National School of Applied Sciences (ENSA) of Agadir, Morocco. His research, in the context of national doctoral thesis, focuses on the thematic of Renewable Energies. The doctoral investigations took place in the Research Team in Laboratory of Engineering Sciences and Energy Management (LASIME), Agadir, Morocco. He can be contacted at email: s.farhat@uiz.ac.ma

Yahya Dbaghi ⓘ 🇬 sc Ⓟ is a Ph.D. student in Electrical Engineering at the EST (High School of Technology), Ibn Zohr University, Agadir, Morocco. He received the master's degree in electrical engineering in 2014 at the faculty of sciences and technologies Marrakech. he is an aggregate professor in electrical engineering in the preparatory classes for Moroccan "Brevet de Technicien Supérieur" since 2016. His research activities include the application of robust control in the renewable energies power systems. The doctoral investigations took place in the Research Team in Engineering Sciences and Energy Management (LASIME) Agadir, Morocco. He can be contacted at email: yahya.dbaghi@edu.uiz.ac.ma.

Diyae Daou ⓘ 🇬 sc Ⓟ is a Ph.D. student in electrical engineering at the ENSA (National school of applied sciences), Ibn Zohr University, Agadir, Morocco. She received Electrical engineering diploma in 2020 at Polytechnique School of Agadir-Universiapolis. Her reaserch, in the context of national doctoral thesis focus on the development and amelioration of numerical solutions dedicated to the integration of renewable energy sources into the electrical grid. The doctoral investigations took place in the Research Team in Engineering Sciences and Energy Management (LASIME) Agadir, Morocco. She can be contacted at email: daoudiyae@gmail.com.